Submitted to Materials Science and Engineering A (2020)

Analysis of the creep behavior of fine-grained AZ31 magnesium alloy

Roberto B. Figueiredo[1,*], Terence G. Langdon[2,3]

[1] Department of Metallurgical and Materials Engineering, Universidade Federal de Minas Gerais, Belo Horizonte, MG 31270-901, Brazil

[2] Materials Research Group, Department of Mechanical Engineering, University of Southampton, Southampton SO17 1BJ, U.K.

[3] Departments of Aerospace & Mechanical Engineering and Materials Science, University of Southern California, Los Angeles, CA 90089-1453, U.S.A.

Abstract

Double-shear creep testing was used to evaluate the creep behavior of a magnesium AZ31 alloy processed by equal-channel angular pressing to produce an average grain size of ~2.7 μm. The results show that rapid creep rates are observed in the early stages of deformation due to the occurrence of grain boundary sliding in the fine-grained structure but the creep rates decrease with increasing deformation due to grain growth. The stress exponent for flow in the early stages is ~2 and the activation energy is ~92 kJ mol^{-1} where these values are consistent with the expectations for grain boundary sliding under superplastic conditions. Annealing the material for 24 h at 723 K before creep testing produces a significantly larger grain size of ~50 μm and this prevents grain boundary sliding and leads to an increasing stress exponent at higher stresses. Deformation mechanism maps are constructed incorporating both the present experimental results for a fine-grained magnesium alloy and results from published data for the AZ31 alloy. These maps provide a useful tool for evaluating the experimental conditions that are necessary for achieving superplastic forming operations.

Keywords: AZ31 magnesium alloy; creep; deformation mechanism maps; equal-channel angular pressing; grain boundary sliding

*corresponding author: figueiredo@demet.ufmg.br (+55) 31 3409-1925

1. Introduction

The high temperature creep behavior of coarse-grained pure magnesium [1] and a magnesium alloy [2] was described in detail in earlier reports. It was shown that the rate controlling mechanism of creep of pure magnesium, with an average grain size of ~80 μm, was dislocation climb up to ~600 – 750 K with dislocation cross-slip at higher temperatures and high stresses but a transition to Nabarro-Herring diffusion creep at these high temperatures and low stresses [1]. The rate-controlling mechanism of creep in a Mg-0.9% Al alloy with an initial grain size of ~240 μm was the viscous glide of dislocations at low stresses and temperatures below ~600 – 750 K but with a transition to dislocation climb at higher stresses [2]. The cross-slip of dislocations from the basal to the prismatic planes was the rate-controlling mechanism at higher temperatures [2].

In later experiments it was shown that experimental data from coarse-grained magnesium alloys with different aluminum contents, including the AZ31 alloy, agreed well at low stresses with viscous glide as the rate-controlling mechanism and a general creep equation was proposed based on the experimental results [3]. It was shown also that experimental data from the AZ31 alloy agreed well with an equation for creep by dislocation climb and a deformation mechanism map was proposed for creep of AZ31 at 673 K considering diffusional and dislocation creep mechanisms and grain boundary sliding [4]. However, a lack of experimental information on the role of grain boundary sliding in the AZ31 alloy prevented a detailed determination of all of the parameters in the creep rate equation.

The development of severe plastic deformation techniques [5] and the use of these procedures for processing magnesium alloys provides an opportunity for studying the high temperature behavior of these alloys having fine or even ultrafine-grained structures. Thus,

processing by equal-channel angular pressing (ECAP) [6] produces exceptionally fine-grained structures in magnesium alloys and this has led to reports of superplastic elongations of more than 1000% in the AZ61 [7] and ZK60 [8, 9] magnesium alloys. It is also now recognized that processing by ECAP produces excellent superplastic properties in the commercial AZ31 alloy [10-14] and an analysis suggests that grain boundary sliding is probably the rate-controlling mechanism [10, 14].

In practice, the AZ31 alloy is a single-phase magnesium alloy and it is anticipated that the absence of a second phase will lead to dynamic grain growth during superplastic deformation at elevated temperatures. The importance of retaining a very small grain size for superplastic flow in magnesium alloys was demonstrated in a recent analysis [15]. Nevertheless, a careful review shows that analyses of the superplastic behavior of this material have focused almost exclusively on the early stages of deformation and there have been no attempts to provide a comprehensive examination of the effect of concurrent grain growth. A recent report suggests that grain growth may play a key role in the high temperature deformation of the AZ31 alloy [16] but a more detailed analysis is necessary to fully document the creep properties. In addition, magnesium alloys processed by ECAP are generally tested using tensile testing whereas many of the early experimental results on conventional superplastic alloys were obtained using double-shear testing in which the application of a constant load is equivalent to a constant stress [17-19].

Accordingly, the present investigation was initiated with two major objectives. First, to obtain a detailed understanding of the creep behavior of a commercial magnesium AZ31 alloy processed by ECAP and then subjected to creep testing under double-shear conditions. Second, to use the experimental data to develop deformation mechanism maps (DMMs) and thereby to provide a detailed overview of the creep properties of the fine-grained AZ31 alloy.

2. Experimental material and procedures

The experiments were conducted using an AZ31 (Mg-3% Al-1% Zn) alloy provided by Timminco Co. (Aurora, CO, U.S.A.) in the form of extruded rods having diameters of 10 mm. The as-received material had an average grain size of ~9.1 μm measured as the mean intercept length. Billets with lengths of 60 mm were cut from the extruded rods using a low-speed diamond-coated saw.

These billets were processed by ECAP using a solid die with an angle, Φ, between the channels of 135º and an external curvature at the intersection of the channels given by an angle, ψ, of 20º. It can be shown that these angles lead to a strain of ~0.46 on each pass through the ECAP die [20]. The die was heated to the required temperature and the temperature was maintained constant throughout processing. The billets were inserted in the die, held for at least 5 minutes before pressing to give temperature homogenization and then the pressing was carried out at a constant rate of punch displacement of ~6 mm s^{-1}. All billets were processed to a total of 6 passes of ECAP using route B_C in which the billet is rotated about the longitudinal axis by 90º between each pass [21]. The first two passes were carried out at 473 K, the following two passes at 443 K and the final two passes at 413 K. The use of temperature reductions in subsequent ECAP passes is an established procedure for minimizing grain growth and achieving optimum superplastic elongations [22].

For double-shear creep testing, cylindrical specimens were machined from the processed billets with diameters of 8 mm and lengths of 34 mm and they were then machined into the form of conventional double-shear creep specimens [23] with diameters and lengths within the symmetrical twin gauge sections of 3 and 2 mm, respectively. These specimens were placed horizontally in a double-shear creep testing machine equipped with a furnace, heated to the

testing temperature and then the temperature was homogenized for 30 minutes before loading. The load was applied by pulling upwards on the central section under conditions of constant stress and the displacement and time were recorded continuously and then converted into shear strain and shear strain rate. Separate tests were conducted at temperatures of 573, 623 and 673 K and the load was varied at selected intervals during testing in order to evaluate the instantaneous strain rate sensitivity.

The microstructures of the material processed by ECAP and after testing in creep were evaluated using conventional metallographic techniques and the spatial grain size, *d*, was calculated as $d = 1.74 \times \overline{L}$ where $\overline{L}$ is the mean linear intercept [17]. A single specimen was also processed by ECAP and then subjected to annealing at 723 K for 24 h to coarsen the grain structure and tested in creep at 573 K under varying loads.

3. Experimental results

3.1 Creep properties after ECAP or annealing

For the samples processed by ECAP, Fig. 1 shows examples of the shear strain, γ, plotted against the time, *t*, when testing at three different temperatures under an applied shear stress of τ = 1.0 MPa. All three curves follow the conventional behavior of an instantaneous strain and an initial primary region where the strain rate decreases with increasing deformation. As anticipated from the creep properties in conventional materials, the strain rate increases with increasing testing temperature.

Figure 2 gives an example of the evolution of the shear strain rate as a function of the shear strain during a test conducted under different applied stresses at a temperature of 623 K. The strain rate decreases initially until reaching a minimum value at a strain of ~1.0 where the minimum creep rate is more than an order of magnitude lower than the initial rate. After reaching

the minimum rate, the stress was abruptly varied periodically and the changes in strain rate were continuously recorded. Using these and other similar data from tests conducted under various stresses at different temperatures, the minimum creep rates, $\dot{\gamma}$, are plotted as a function of the shear stress in Fig. 3 for a series of tests carried out at 573, 623 and 673 K in the samples processed by ECAP (upper points) and in a test conducted at 573 K for the material subjected to ECAP and subsequent annealing (lower points). The creep rates for the material processed by ECAP exhibit a stress exponent of ~2 while the material subjected to annealing after ECAP processing exhibits a different trend with an increase in the stress exponent at higher stresses.

3.2 Microstructural evolution in the AZ31 alloy

The specimens processed by ECAP exhibited average grain sizes of ~1.7 μm and the single specimen annealed for 24 h at 723 K had an average grain size of ~50 μm. This demonstrates the ability of ECAP to introduce significant grain refinement and, in the absence of a second phase or any significant precipitates, the overall lack of thermal stability in the AZ31 alloy at elevated temperatures.

Figure 4 shows images of the grain structures of the AZ31 alloy (a) processed by ECAP and after creep testing at (b) 573, (c) 623 and (d) 673 K. As anticipated, the grain size increases with increasing testing temperature and the average values are ~12, ~20 and ~27 μm after creep testing at 573, 623 and 673 K respectively. These results confirm the lack of thermal stability and the occurrence of significant grain growth during the creep testing.

Earlier reports [13, 14, 24, 25] showed that this alloy develops significant cavitation during high temperature stretching which ultimately produces fracture in this material. Moreover, it was shown that finer grain sizes lead to lower area fractions of cavities. As a consequence, finer grain structures are associated with higher elongations. It was shown that

ECAP processing parameters similar to those used in the present experiments are able to produce significant grain refinement and elongations up to ~1200% in tension were achieved in this material [14].

4. Discussion

4.1. Creep deformation mechanism of the material processed by ECAP

The general creep behavior of metals is described by a rate-controlling equation of the form [26]

$$\dot{\varepsilon} = \frac{AGb}{kT} D_0 \exp\left(\frac{-Q}{RT}\right)\left(\frac{b}{d}\right)^p \left(\frac{\sigma}{G}\right)^n \quad (1)$$

where A is a dimensionless constant, G is the shear modulus, b is the Burgers vector modulus, k is Boltzmann's constant, T is the absolute temperature, D_0 is a frequency factor, Q is the activation energy, R is the gas constant, d is the grain size, σ is the applied stress, p is the inverse grain size exponent and n is the stress exponent. The activation energy, Q, can be estimated from the variation of the creep rate with the inverse of temperature provided the applied stress and the grain size are maintained constant. Figure 5 shows a plot of the variation of the normalized shear strain rate as a function of the inverse of temperature for tests conducted with a shear stress of 1.0 MPa, where these creep data were plotted as the shear strain rate against shear strain and then extrapolated to zero strain. This procedure was adopted in order to minimize the effect of grain growth that takes place during creep deformation. It is apparent that the data exhibit a linear trend and the slope gives an activation energy of ~92 kJ mol^{-1} which is in excellent agreement with the expected activation energy for grain boundary diffusion in magnesium [27].

The stress exponent of $n \approx 2$ obtained from the creep tests of the material processed by ECAP (Fig. 3) and the activation energy of $Q \approx 92$ kJ mol^{-1} calculated at different creep

temperatures (Fig. 5) are both in agreement with a mechanism of grain boundary sliding [28] which was also reported earlier during high temperature tensile testing of the AZ31 alloy processed by ECAP [10, 14]. In order to determine whether the present creep data agree with the theoretical prediction for grain boundary sliding, the shear strain rate, $\dot{\gamma}$, was transformed to the effective strain rate, $\dot{\varepsilon}$, using the relation $\dot{\varepsilon} = \dot{\gamma}/\sqrt{3}$ and the shear stress, τ, was transformed to the effective stress, σ, by taking $\sigma = \tau \times \sqrt{3}$. The minimum effective strain rates calculated from the tests at different temperatures were normalized by the effect of temperature and grain size by considering a grain size exponent of $p \approx 2$ as in conventional grain boundary sliding [28] and the results were then plotted as a function of the normalized stress, σ/G, as in Fig. 6. The grain sizes determined after creep testing were used in the calculations in order to take the grain growth effect into account. Consistent with this plot, it is important to note that an earlier report on high temperature testing of the AZ31 alloy reported experimental evidence for $p \approx 2$ during grain boundary sliding [14]. The theoretical prediction for grain boundary sliding is also shown by the solid line in Fig. 6 labelled $\dot{\varepsilon}_{GBS}$. Generally, it is observed that the data for the creep tests of the material processed by ECAP follow a similar trend and with a good agreement with the theoretical relationship except only for the datum point at the lowest stress for the test at 573 K (shown by the square in Fig. 6) which is slightly below the predicted value. Also, it is apparent that the ECAP and annealed material (shown by the inverted triangles in Fig. 6) follows a different trend with lower creep rates than those predicted by the grain boundary sliding mechanism.

4.2. Analysis of creep mechanisms in the AZ31 alloy

An earlier report [29] described the occurrence of Nabarro-Herring creep [30, 31] in pure magnesium with a grain size of 80 μm at 698 K at stresses lower than 1.4 MPa and, in addition,

decreasing the temperature to 543 K and the grain size to 50 μm gave Coble creep [32] at stresses below 2.8 MPa. Thus, lower temperatures and smaller grain sizes favor Coble creep instead of Nabarro-Herring creep. Furthermore, Nabarro-Herring creep was also reported at 773 K in pure magnesium with a grain size of 80 μm at stresses lower than ~2.5 MPa [1]. It is appropriate, therefore, to examine the significance of diffusional creep in the present experiments.

The rate equations for Nabarro-Herring and Coble creep may be expressed in the form of eq. 1 as

$$\dot{\varepsilon}_{Nab-Her} = 14\frac{D_L Gb}{kT}\left(\frac{b}{d}\right)^2\left(\frac{\sigma}{G}\right)^1 \quad (2)$$

and

$$\dot{\varepsilon}_{Coble} = 66.8\frac{D_{gb} Gb}{kT}\left(\frac{b}{d}\right)^3\left(\frac{\sigma}{G}\right)^1 \quad (3)$$

where D_L is the coefficient for lattice diffusion and D_{gb} is the coefficient for grain boundary diffusion.

Grain boundary sliding has been reported in magnesium alloys including AZ31 [10, 14] and this is associated with high elongations in tension with a rate-controlling relationship given by [26]

$$\dot{\varepsilon}_{GBS} = 5\frac{\delta D_{gb} G}{kT}\left(\frac{b}{d}\right)^2\left(\frac{\sigma}{G}\right)^2 \quad (4)$$

where δ is the grain boundary width equal to ~2*b* [10].

The occurrence of dislocation glide is also a potential creep mechanism in the AZ31 alloy where the viscous glide of dislocations drag aluminum solutes at low stresses but, as in the conventional creep of solid solution alloys [33, 34], there is a transition from control by viscous

glide to dislocation climb with increasing stress. An empirical relationship for the viscous glide of dislocations in Mg-Al alloys was proposed earlier [3] and this may be adapted to fit the format of eq. 1 so that the relationship becomes

$$\dot{\varepsilon} = 0.04 \frac{\tilde{D}Gb}{kT}\left(\frac{\sigma}{G}\right)^3 \quad (5)$$

where $\tilde{D}$ is the coefficient for aluminum diffusion within the magnesium matrix.

Finally, following the analysis presented earlier [33], a creep relationship was derived to predict the creep rate where dislocation climb becomes the rate-controlling mechanism:

$$\dot{\varepsilon}_C = A_{climb}\left\{\frac{\gamma_{SF}}{Gb}\right\}^3 \frac{D_L Gb}{kT}\left(\frac{\sigma}{G}\right)^5 \quad (6)$$

where γ_{SF} is the stacking fault energy and A_{climb} is a constant. Later, it was shown that the best agreement with experimental data for magnesium alloys is achieved by using $A_{climb} = 3.6 \times 10^{11}$ [4].

In order to investigate the agreement between the theoretical creep rate models and the measured experimental creep rates, data were collected from various reports where tests were conducted at similar temperatures as in the present experiments: thus, data were used where the testing temperatures were 573, 623 and 673 K. Table 1 provides a summary of reports of high temperature deformation for the AZ31 alloy including the testing temperature, the grain size and the reported creep mechanism.

Using these various reports, Fig. 7 shows the experimental data plotted as creep rate against stress for tests conducted at temperatures of (a) 573, (b) 623 and (c) 673 K. The creep rates predicted by the theoretical models are also shown in Fig. 7 using continuous lines for the dislocation creep mechanisms (climb and viscous glide) and dashed lines for creep mechanisms which depend on grain size (Coble creep and grain boundary sliding). Table 2 shows the values

of the various parameters used in the calculations for the theoretical creep rates. The agreement between the theoretical predictions and the experimental data is generally very good. Thus, the creep behavior of coarse-grained AZ31 alloy agrees well with the dislocation creep mechanisms (viscous glide and climb-controlled creep) while the fine-grained AZ31 alloy exhibits grain boundary sliding with some evidence for transitions at the lowest stresses. The creep rates observed in the present experiments in the material subjected to ECAP and annealing agree well with the predicted rates for climb-controlled creep at high stresses, viscous glide creep at intermediate stresses and with some evidence for Coble creep at the lowest stresses. The grain size in this material was ~50 μm and this grain size is too coarse to observe grain boundary sliding under the present experimental conditions.

4.3. Deformation mechanism maps for the AZ31 alloy

This analysis demonstrates very good agreement between the theoretical creep predictions and the experimental data both from the present experiments and from published reports. The only creep mechanism not documented in the AZ31 alloy is Nabarro-Herring diffusion creep although it was reported earlier in pure magnesium [1, 29]. Also, the present results show that grain boundary sliding is not a viable mechanism in the AZ31 alloy with a grain size of 50 μm although an earlier report recorded a contribution from this mechanism in samples with a grain size of 40 μm [37]. Accordingly, it is important to construct deformation mechanism maps using eqs. 2-6 and the parameters in Table 2 in order to fully delineate the ranges of stress and grain size associated with the different creep mechanisms. These parameters are associated with pure Mg except for the stacking fault energy where the value for the Mg-3% Al alloy was used [4]. To provide consistency with the available experimental data, a grain size of 40 μm was considered as the limiting size for the occurrence of grain boundary sliding.

Figure 8 shows maps of normalized grain size versus normalized stress for temperatures of (a) 573, (b) 623 and (c) 673 K. Different colors are used for each creep mechanism with red for climb-controlled creep, blue for viscous glide, yellow for grain boundary sliding, green for Coble creep and cyan for Nabarro-Herring creep. Experimental points are plotted using color-filled symbols using the same association between creep mechanism and colors which was used for the DMM. Comparing the data in the DMMs and the creep mechanisms reported in Table 1 reveals good agreement between the theoretical predictions and experimental observations. The maps show that Nabarro-Herring creep is only expected at very low stresses in coarse-grained material which explains the lack of reports of this creep mechanism in the AZ31 alloys.

Careful inspection of the data in the literature and the DMM predictions reveals small discrepancies in the stress levels for the transitions from grain boundary sliding to dislocation creep. These differences are attributed to the formation of sub-grain structures which restrict the accommodation by intragranular slip of the grain boundary sliding mechanism. The equation relating the equilibrium sub-grain size, λ, to the applied stress is given, for both metals [41] and ceramics [42], by the relationship

$$\frac{\lambda}{b} = 20\left(\frac{G}{\sigma}\right) \qquad (7)$$

It was shown earlier that superplasticity may be achieved in metals when the grain size is smaller than the sub-grain size so that there are no barriers to dislocation movement within the grains [43] and this transition is illustrated in Fig. 8 by plotting, at lower right in each DMM, eq. 7 with $d = \lambda$. These plots show that the experimental datum points span the boundaries where subgrain formation becomes important and this may lead to transitions to dislocation creep at stresses which are lower than expected. In fact, a coexistence between grain boundary sliding and dislocation creep was recently reported in an AZ31 alloy with a grain size of 16 μm at a stress of

10 MPa at 573 K [44]. Careful inspection of the DMM for this temperature shows that this grain size and stress fall in the region for GBS but the grain size is larger than the predicted subgrain size.

Finally, there is a current interest in using the AZ31 alloy for superplastic forming operations [45-47]] but this will require operating within the regime of grain boundary sliding where $d < \lambda$ so that no sub-grain boundaries are formed within the grains [43]. The DMMs presented in Fig. 8 provide a useful tool for delineating the stresses and grain sizes that are required in order to achieve superplastic properties at selected temperatures within the range from 573 to 673 K.

5. Summary and conclusions

1- A commercial magnesium AZ31 alloy was processed by ECAP to produce a grain size of ~2.7 μm and then tested in creep at 573, 623 and 673 K at stresses in the range from 0.5 to 12.6 MPa using a double-shear creep testing facility. One sample was subjected to ECAP, annealed for 24 h at 723 K to produce a grain size of ~50 μm and then creep tested under different stresses at 573 K. The results from these tests were compared with theoretical predictions for different creep mechanisms.

2- An analysis of the creep behavior of the ECAP-processed samples revealed significant grain growth during testing with an initial stress exponent of ~2 and an activation energy of ~92 kJ mol^{-1} which is similar to the values expected for grain boundary diffusion. The rate-controlling mechanism is attributed to grain boundary sliding in this fine-grained material. For the annealed material, the stress exponents were larger due to the occurrence of viscous glide and dislocation climb.

3- Deformation mechanism maps were constructed by considering the available data for high temperature deformation of the fine-grained AZ31 alloy and by using a limiting grain size for grain boundary sliding. The maps include datum points from a wide range of experimental reports.

Acknowledgements

The authors acknowledge support from FAPEMIG, CAPES, CNPq and the European Research Council under ERC Grant Agreement No. 267464-SPDMETALS.

Data availability statement

The raw/processed data required to reproduce these findings cannot be shared at this time due to technical or time limitations.

References

[1] S.S. Vagarali, T.G. Langdon, Deformation mechanisms in h.c.p. metals at elevated temperatures—I. Creep behavior of magnesium, Acta Metallurgica 29(12) (1981) 1969-1982.
[2] S.S. Vagarali, T.G. Langdon, Deformation mechanisms in h.c.p. metals at elevated temperatures—II. Creep behavior of a Mg-0.8% Al solid solution alloy, Acta Metallurgica 30(6) (1982) 1157-1170.
[3] H. Watanabe, H. Tsutsui, T. Mukai, M. Kohzu, S. Tanabe, K. Higashi, Deformation mechanism in a coarse-grained Mg–Al–Zn alloy at elevated temperatures, International Journal of Plasticity 17(3) (2001) 387-397.
[4] H. Somekawa, K. Hirai, H. Watanabe, Y. Takigawa, K. Higashi, Dislocation creep behavior in Mg–Al–Zn alloys, Materials Science and Engineering: A 407(1) (2005) 53-61.
[5] R.Z. Valiev, R.K. Islamgaliev, I.V. Alexandrov, Bulk nanostructured materials from severe plastic deformation, Progress in Materials Science 45 (2000) 103-187.
[6] R.Z. Valiev, T.G. Langdon, Principles of equal-channel angular pressing as a processing toold for grain refinement, Progress in Materials Science 51 (2006) 881-981.
[7] Y. Miyahara, Z. Horita, T.G. Langdon, Exceptional superplasticity in an AZ61 magnesium alloy processed by extrusion and ECAP, Materials Science and Engineering: A 420(1) (2006) 240-244.
[8] R. Lapovok, R. Cottam, P.F. Thomson, Y. Estrin, Extraordinary superplastic ductility of magnesium alloy ZK60, Journal of Materials Research 20(6) (2005) 1375-1378.
[9] R.B. Figueiredo, T.G. Langdon, Record superplastic ductility in a magnesium alloy processed by equal-channel angular pressing, Advanced Engineering Materials 10(1-2) (2008) 37-40.
[10] R.B. Figueiredo, T.G. Langdon, Developing superplasticity in a magnesium AZ31 alloy by ECAP, Journal of Materials Science 43(23-24) (2008) 7366-7371.
[11] H.K. Lin, J.C. Huang, T.G. Langdon, Relationship between texture and low temperature superplasticity in an extruded AZ31 Mg alloy processed by ECAP, Materials Science and Engineering: A 402(1) (2005) 250-257.
[12] R. Lapovok, Y. Estrin, M.V. Popov, T.G. Langdon, Enhanced superplasticity in a magnesium alloy processed by equal-channel angular pressing with a back-pressure, Advanced Engineering Materials 10(5) (2008) 429-433.
[13] R.B. Figueiredo, T.G. Langdon, Influence of rolling direction on flow and cavitation in a superplastic magnesium alloy processed by equal-channel angular pressing, Materials Science and Engineering A 556 (2012) 211-220.
[14] R.B. Figueiredo, T.G. Langdon, Evaluating the superplastic flow of a magnesium AZ31 alloy processed by equal-channel angular pressing, Metallurgical and Materials Transactions A: Physical Metallurgy and Materials Science 45(8) (2014) 3197-3204.
[15] M. Kawasaki, R.B. Figueiredo, T.G. Langdon, The requirements for superplasticity with an emphasis on magnesium alloys, Advanced Engineering Materials 18(1) (2016) 127-131.
[16] S. Spigarelli, O.A. Ruano, M. El Mehtedi, J.A. del Valle, High temperature deformation and microstructural instability in AZ31 magnesium alloy, Materials Science and Engineering: A 570 (2013) 135-148.
[17] F.A. Mohamed, T.G. Langdon, Creep at low stress levels in the superplastic Zn-22% Al eutectoid, Acta Metallurgica 23(1) (1975) 117-124.

[18] F.A. Mohamed, T.G. Langdon, Creep behaviour in the superplastic Pb–62% Sn eutectic, The Philosophical Magazine: A Journal of Theoretical Experimental and Applied Physics 32(4) (1975) 697-709.
[19] F.A. Mohamed, S.-A. Shei, T.G. Langdon, The activation energies associated with superplastic flow, Acta Metallurgica 23(12) (1975) 1443-1450.
[20] Y. Iwahashi, J. Wang, Z. Horita, M. Nemoto, T.G. Langdon, Principle of equal-channel angular pressing for the processing of ultra-fine grained materials, Scripta Materialia 35(2) (1996) 143-146.
[21] M. Furukawa, Y. Iwahashi, Z. Horita, M. Nemoto, T.G. Langdon, The shearing characteristics associated with equal-channel angular pressing, Materials Science and Engineering A 257(2) (1998) 328-332.
[22] S. Lee, P.B. Berbon, M. Furukawa, Z. Horita, M. Nemoto, N.K. Tsenev, R.Z. Valiev, T.G. Langdon, Developing superplastic properties in an aluminum alloy through severe plastic deformation, Materials Science and Engineering: A 272(1) (1999) 63-72.
[23] H. Kim, F. Mohamed, J. Earthman, A novel specimen geometry for double shear creep experiments, Journal of Testing and Evaluation 19(2) (1991) 93-96.
[24] R.B. Figueiredo, T.G. Langdon, Characteristics of cavitation in a superplastic magnesium AZ31 alloy processed by equal-channel angular pressing, Reviews on Advanced Materials Science 25(3) (2010) 249-255.
[25] R.B. Figueiredo, S. Terzi, T.G. Langdon, Using X-ray microtomography to evaluate cavity formation in a superplastic magnesium alloy processed by equal-channel angular pressing, Acta Materialia 58(17) (2010) 5737-5748.
[26] T.G. Langdon, An analysis of flow mechanisms in high temperature creep and superplasticity, Materials Transactions 46(9) (2005) 1951-1956.
[27] H.J. Frost;, M.F. Ashby, Deformation-Mechanism Maps: The Plasticity and Creep of Metals and Ceramics, Pergamon Press1982.
[28] T.G. Langdon, A unified approach to grain boundary sliding in creep and superplasticity, Acta Metallurgica et Materialia 42(7) (1994) 2437-2443.
[29] R.B. Jones, Diffusion creep in polycrystalline magnesium, Nature 207(4992) (1965) 70-70.
[30] F.R.N. Nabarro, Deformation of crystals by the motion of single ions., Report of a conference on strength of solids, The Physical Society, London, U.K., 1948, pp. 75-90.
[31] C. Herring, Diffusional viscosity of a polycrystalline solid, Journal of Applied Physics 21(5) (1950) 437-445.
[32] R.L. Coble, A model for boundary diffusion controlled creep in polycrystalline materials, Journal of Applied Physics 34(6) (1963) 1679-1682.
[33] F.A. Mohamed, T.G. Langdon, The transition from dislocation climb to viscous glide in creep of solid solution alloys, Acta Metallurgica 22(6) (1974) 779-788.
[34] P. Yavari, T.G. Langdon, An examination of the breakdown in creep by viscous glide in solid solution alloys at high stress levels, Acta Metallurgica 30(12) (1982) 2181-2196.
[35] K. Kitazono, E. Sato, K. Kuribayashi, Internal stress superplasticity in polycrystalline AZ31 magnesium alloy, Scripta Materialia 44(12) (2001) 2695-2702.
[36] X. Wu, Y. Liu, Superplasticity of coarse-grained magnesium alloy, Scripta Materialia 46(4) (2002) 269-274.
[37] J.A. del Valle, M.T. Pérez-Prado, O.A. Ruano, Deformation mechanisms responsible for the high ductility in a Mg AZ31 alloy analyzed by electron backscattered diffraction, Metallurgical and Materials Transactions A 36(6) (2005) 1427-1438.

[38] H. Watanabe, M. Fukusumi, Mechanical properties and texture of a superplastically deformed AZ31 magnesium alloy, Materials Science and Engineering: A 477(1) (2008) 153-161.
[39] S. Spigarelli, M. El Mehtedi, D. Ciccarelli, M. Regev, Effect of grain size on high temperature deformation of AZ31 alloy, Materials Science and Engineering: A 528(22) (2011) 6919-6926.
[40] M.L. Olguín-González, D. Hernández-Silva, M.A. García-Bernal, V.M. Sauce-Rangel, Hot deformation behavior of hot-rolled AZ31 and AZ61 magnesium alloys, Materials Science and Engineering: A 597 (2014) 82-88.
[41] J.E. Bird, A.K. Mukherjee, J.E. Dorn, Quantitative Relation Between Properties and Microstructure, Israel Universities Press, Jerusalem, Israel, 1969.
[42] W.R. Cannon, T.G. Langdon, Creep of ceramics, Journal of Materials Science 23(1) (1988) 1-20.
[43] F.A. Mohamed, T.G. Langdon, Deformation mechanism maps for superplastic materials, Scripta Metallurgica 10(8) (1976) 759-762.
[44] T. Dessolier, P. Lhuissier, F. Roussel-Dherbey, F. Charlot, C. Josserond, J.-J. Blandin, G. Martin, Effect of temperature on deformation mechanisms of AZ31 Mg-alloy under tensile loading, Materials Science and Engineering: A 775 (2020) 138957.
[45] M.K. Khraisheh, F.K. Abu-Farha, M.A. Nazzal, K.J. Weinmann, Combined mechanics-materials based optimization of superplastic forming of magnesium AZ31 alloy, CIRP Annals 55(1) (2006) 233-236.
[46] M.K. Khraisheh, F.K. Abu-Farha, K.J. Weinmann, Investigation of post-superplastic forming properties of AZ31 magnesium alloy, CIRP Annals 56(1) (2007) 289-292.
[47] M. Cusick, F. Abu-Farha, P. Lours, Y. Maoult, G. Bernhart, M. Khraisheh, Superplastic forming of AZ31 magnesium alloy with controlled microstructure, Materialwissenschaft und Werkstofftechnik 43(9) (2012) 810-816.

Figure(s)

Table 1 – Summary of creep data for the AZ31 alloy from the present experiments and from other reports.

T (K)	d (μm)	Creep mechanism	Reference
573, 623, 673	12, 20, 27	Grain boundary sliding	Present results
573	50	Dislocation climb, viscous glide and Coble creep	Present results
573, 623, 673, 723	85	Viscous glide	[35]
598, 623, 648, 673	130	Viscous glide at low strain rates	[3]
623, 673, 723, 773	300 / 25	Viscous glide at strain rates lower than 10^{-3} s^{-1}	[36]
473, 523, 573	56	Climb-controlled dislocation creep	[4]
573, 648	17, 40	Grain boundary sliding at low strain rates and climb-controlled creep at high strain rates	[37]
623, 673, 723	10, 18	Grain boundary sliding at low strain rates and dislocation creep at higher strain rates.	[10]
673, 723	27	Grain boundary sliding at strain rates $<6 \times 10^{-5}$ s^{-1} and dislocation creep at higher strain rates.	[38]
673	17	Grain boundary sliding at low strain rates and slip creep at high strain rates.	[16]
573	22	Viscous glide at low strain rates and climb at high strain rates.	[39]
623	7.7	Grain boundary sliding	[14]
673, 723, 773	23*, 42*	Glide controlled dislocation creep	[40]

*The grain size was calculated as $d = 1.74 \times \overline{L}$, where $\overline{L}$ is the mean linear intercept length.

Table 2 – Parameters used in calculations of creep properties in Figs 7 and 8.

Parameter	Value	Reference
G	(19,200-8.6T) MPa	[2]
b	3.2×10^{-10} m	[27]
δ	6.4×10^{-10} m	[10]
γ_{SF}	27.8 mJ m^{-2}	[4]
D_L	10^{-4} exp (-135,000/RT) m^2 s^{-1}	[27]
D_{gb}	$(5 \times 10^{-12}/\delta)$ exp (-92,000/RT) m^2 s^{-1}	[27]
$\tilde{D}$	1.2×10^{-3} exp (-143,000/RT) m^2 s^{-1}	[2]

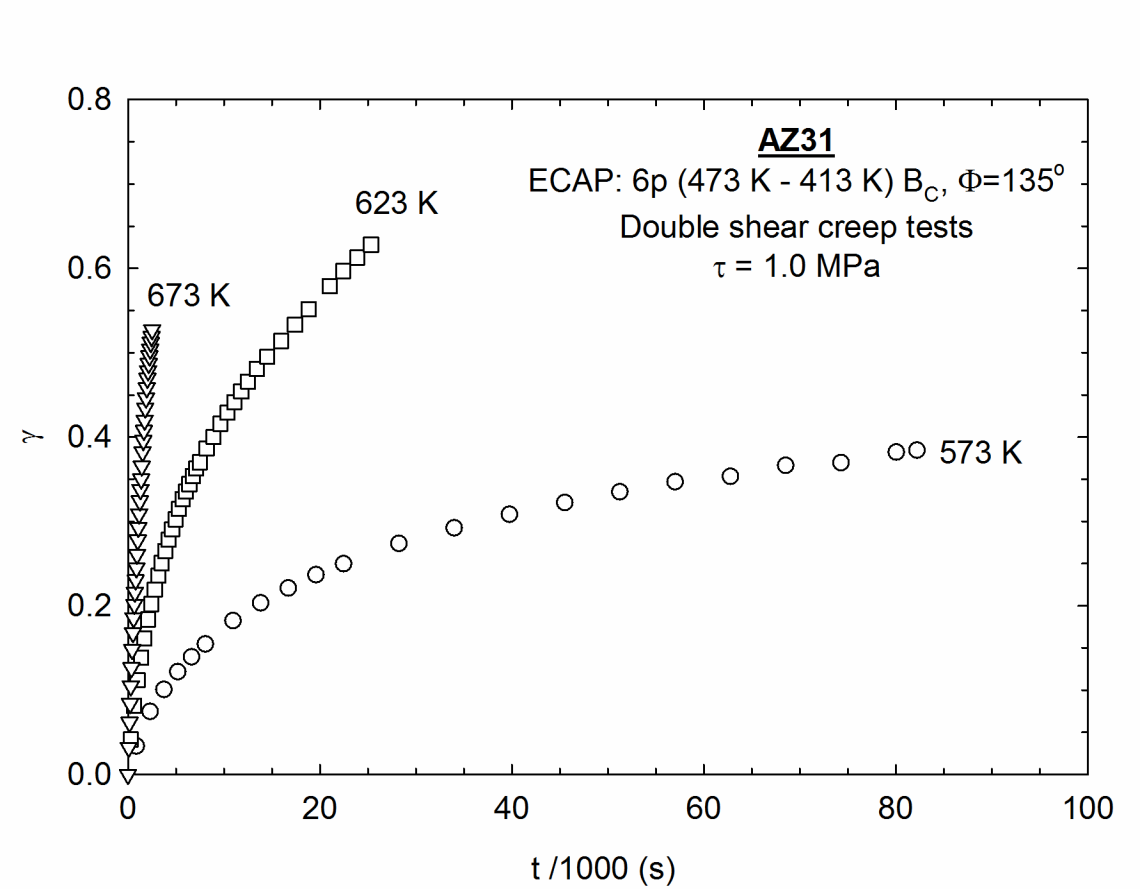

Figure 1 – Shear strain plotted as a function of the time for creep testing of the material processed by ECAP and tested under a shear stress of 1.0 MPa at 573, 623 and 673 K.

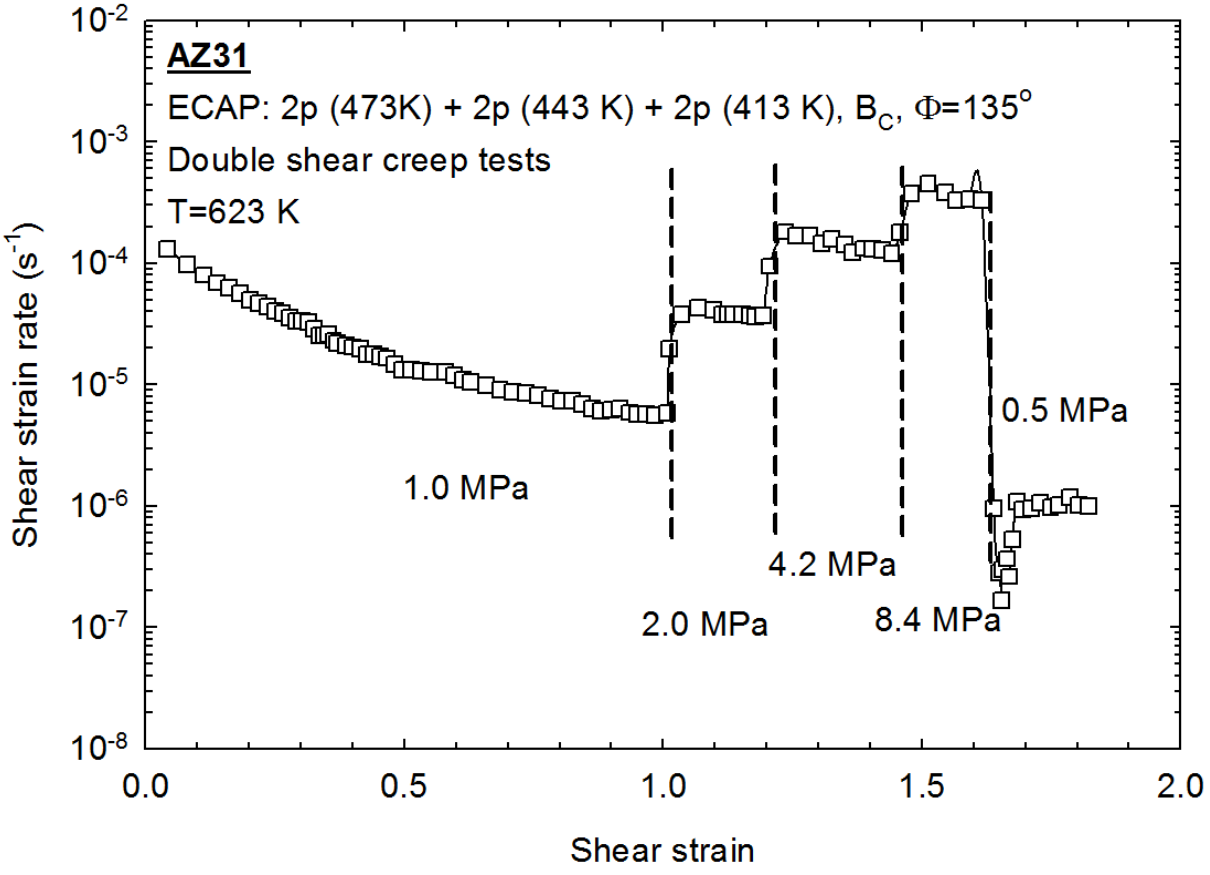

Figure 2 – Shear strain rate plotted as a function of shear strain during creep testing at 623 K with different levels of applied shear stress.

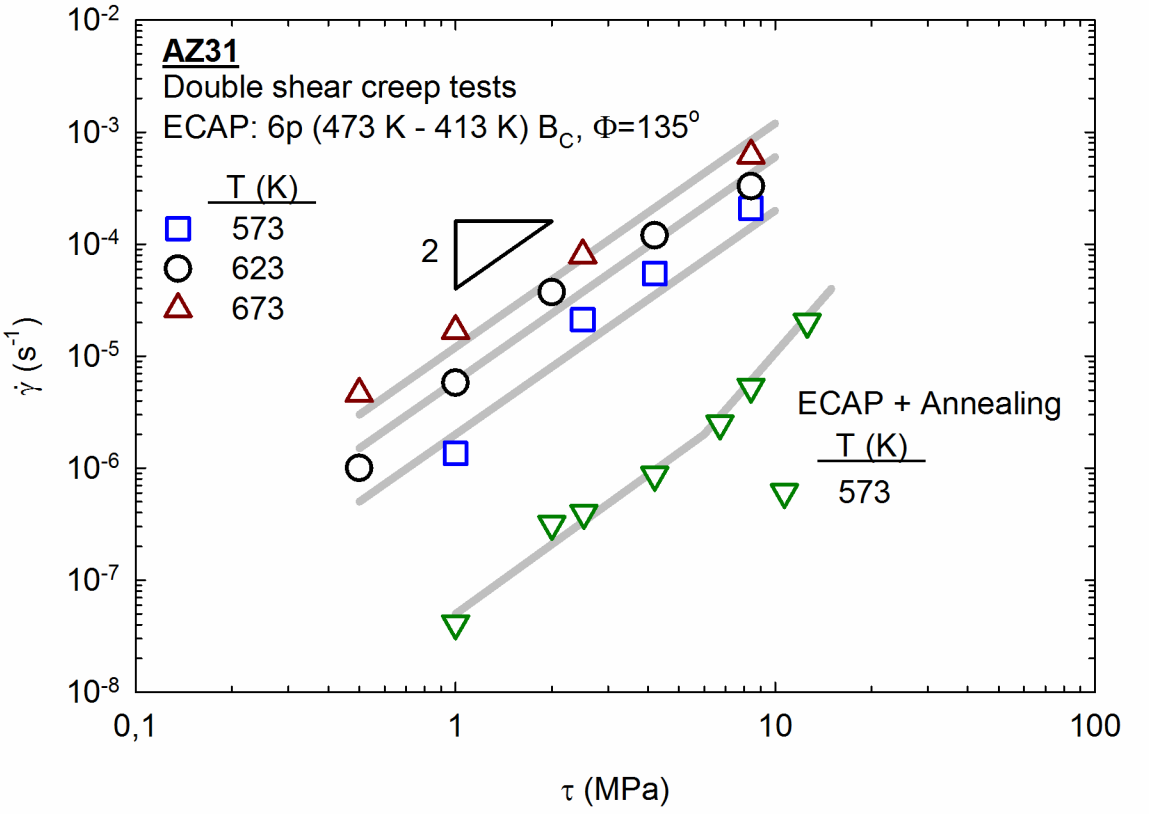

Figure 3 – Minimum creep rates plotted as a function of the applied stress for tests conducted at 573, 623 and 673 K.

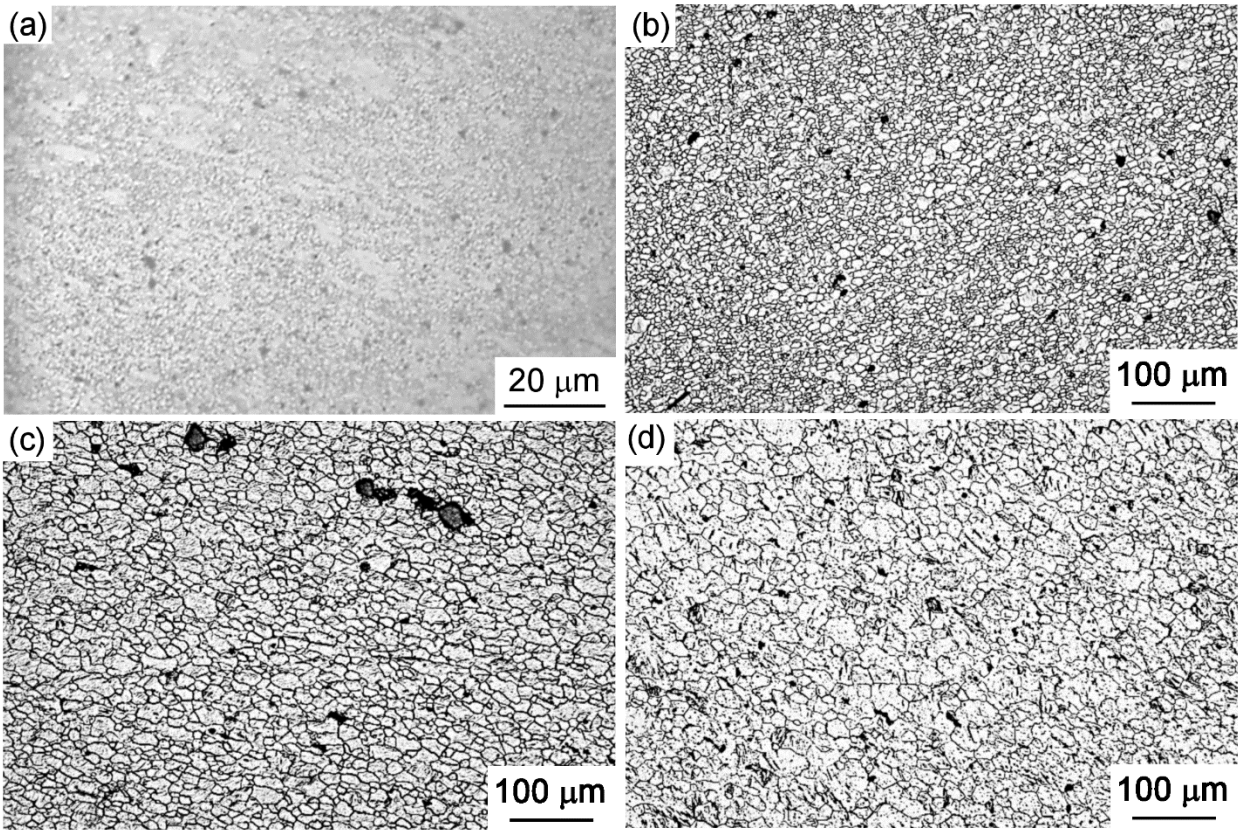

Figure 4 – Representative images of the grain structures of the AZ31 magnesium alloy (a) processed by ECAP and tested in creep at (b) 573, (c) 623 and (d) 673 K.

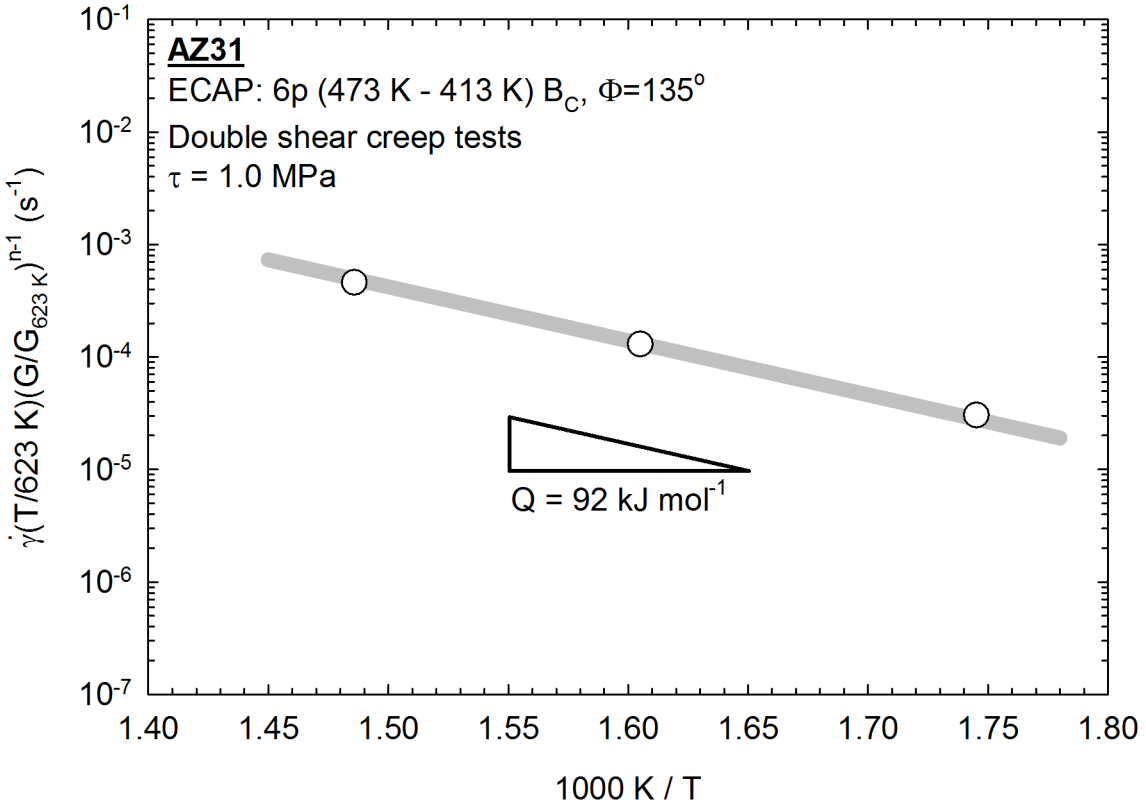

Figure 5 – Creep rates extrapolated to zero strain normalized by the difference in creep testing temperature and plotted as a function of the inverse of the absolute temperature in order to determine an activation energy for creep.

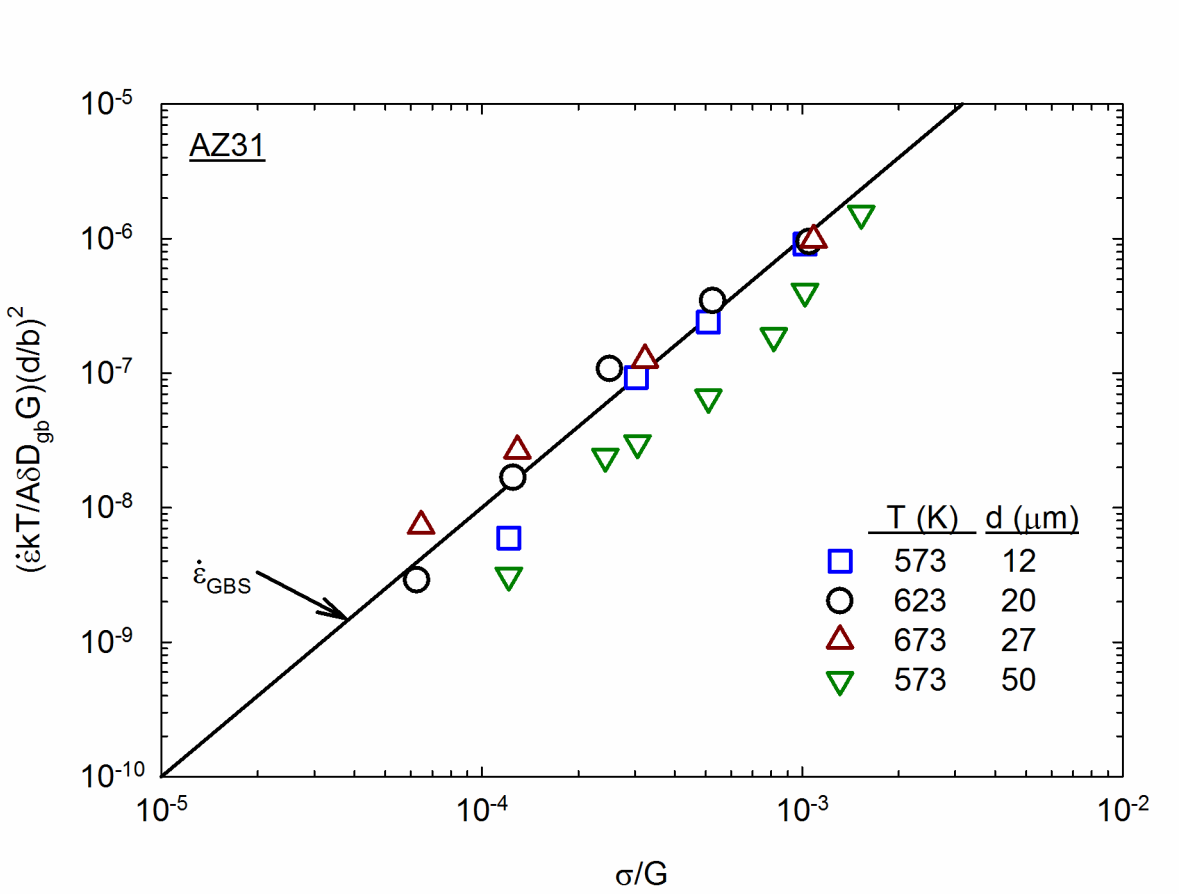

Figure 6 – Effective creep rates normalized by the effect of grain size and temperature and plotted as a function of the effective stress normalized by the shear modulus: the theoretical prediction for grain boundary sliding [28] is also shown for comparison.

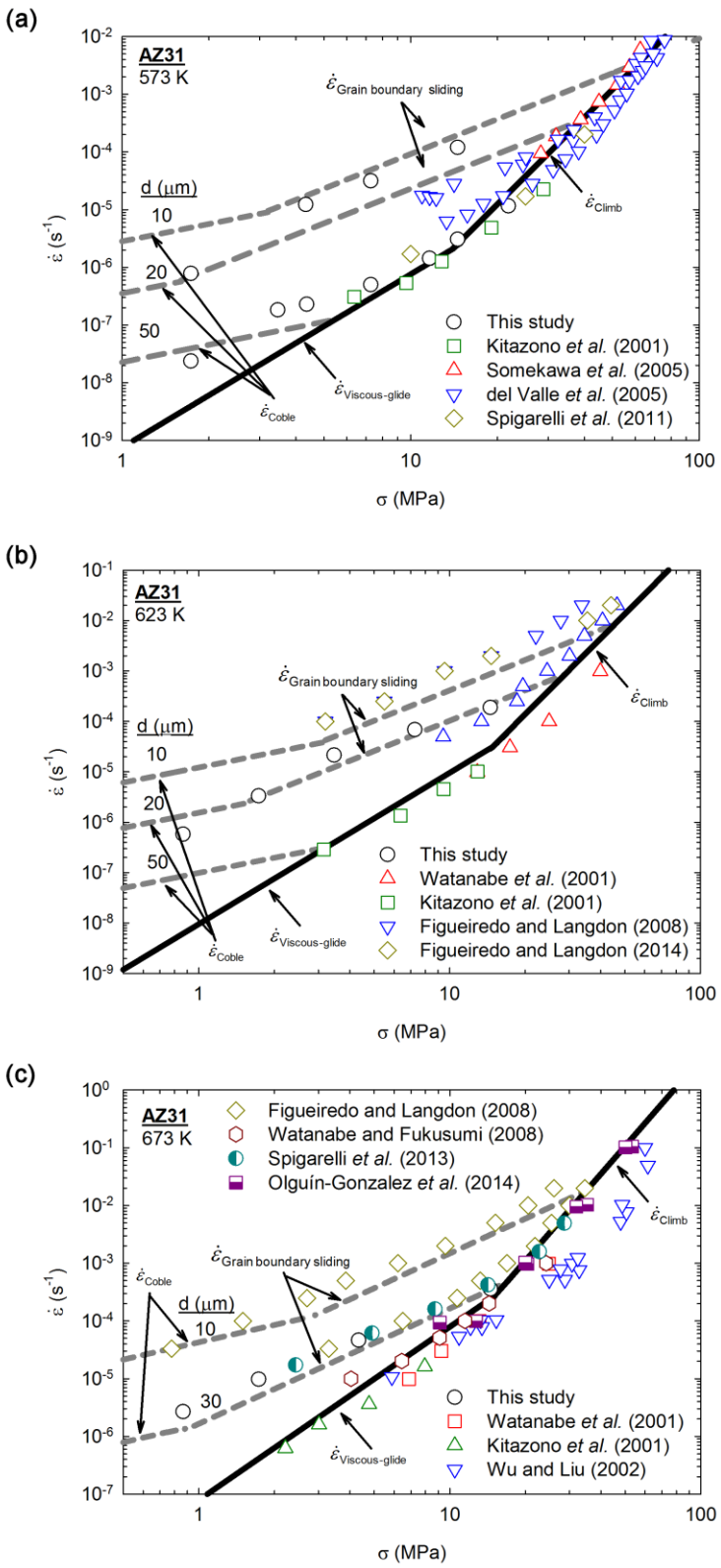

Figure 7 – Effective creep rates plotted as a function of the effective stress for testing at (a) 573, (b) 623 and (c) 673 K: data from published reports [3,4,10,14,16, 35-40] and theoretical predictions for different creep mechanisms are also shown for comparison.

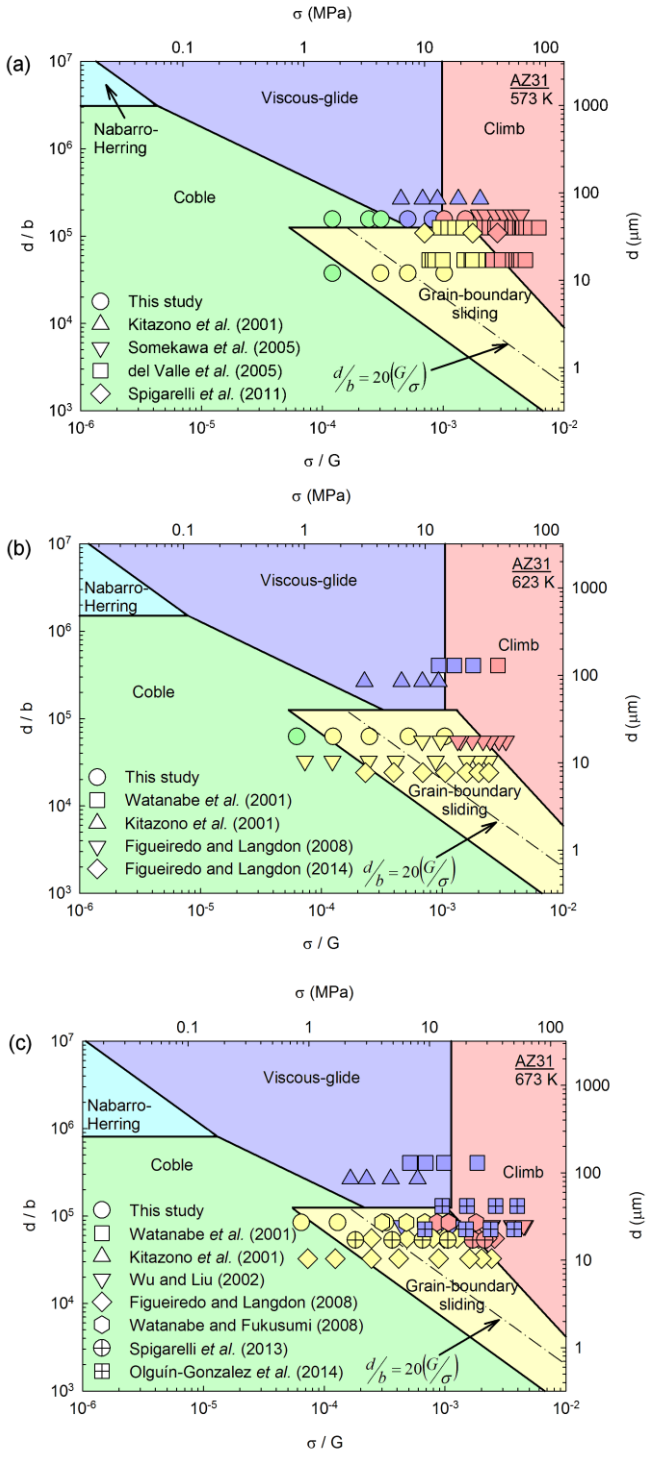

Figure 8 – Deformation mechanism maps for creep of AZ31 alloy at (a) 573 K, (b) 623 K and (c) 673 K. Data from the present experiments and the literature [3,4,10,14,16, 35-40] are also shown for comparison.